Journal of Alloys and Compounds 517 (2012) 54–60

Contents lists available at SciVerse ScienceDirect

Journal of Alloys and Compounds

journal homepage: www.elsevier.com/locate/jallcom

Influence of anionic concentration and deposition temperature on formation of wurtzite CdS thin films by in situ chemical reaction method

Juan Chu [a], Zhengguo Jin [a,*], Weidong Wang [a], Hui Liu [a], Dalong Wang [a], Jingxia Yang [b], Zhanglian Hong [b]

[a] School of Materials Science and Engineering, Key Laboratory for Advanced Ceramics and Machining Technology of Ministry of Education, Tianjin University, Tianjin 300072, PR China
[b] State Key Laboratory of Silicon Materials, Department of Materials Science & Engineering, Zhejiang University, Hangzhou 310027, PR China

ARTICLE INFO

Article history:
Received 7 October 2011
Received in revised form
23 November 2011
Accepted 28 November 2011
Available online 9 December 2011

Keywords:
In situ synthesis
CdS nanocrystalline thin films
Molar concentration
Deposition temperature
Annealing treatment

ABSTRACT

Nanocrystalline CdS thin films were deposited on glass substrates by a new in situ chemical reaction synthesis using cadmium precursor solid films as reaction source and sodium sulfide based solutions as anionic reaction medium. The influence of the S:Cd molar concentrations in separate cationic and anionic precursor solutions and the deposition temperature on the crystallized structure, morphologies, chemical component and optical properties of the deposited CdS films was investigated by X-ray diffraction, field emission scanning electron microscope, energy dispersive X-ray analysis and UV–Vis spectra measurements. The results show that CdS thin films deposited by the in situ chemical reaction synthesis have wurtzite structure with (0 0 2) plane preferential orientation and this tendency gradually enhances with increase of S:Cd molar concentration ratio. The deposition rate was 80–100 nm thickness per cycle in the range of deposition temperature from 20 °C to 60 °C.

1. Introduction

In the last two decades, a large amount of work has been devoted to study of CdS thin films for their capacity to increase the conversion coefficient of solar cell devices [1–5] and potential in wide applications relating to the ability to adjust electronic band gap energy through particle size [6]. CdS is an n-type semiconductor which has direct band gap (E_g = 2.42 eV) and optical absorption suitable for photovoltaic applications as window coatings in many types of solar cells with absorber materials such as Cu(In, Ga)Se_2 [7], CdTe [8,9] or $CuInSe_2$ [10,11]. Furthermore, CdS nanocrystals are applied for lasers [12], biological labels [13,14], photoconducting cells in sensors [15] and photoelectrocatalysis devices [16–19].

Numerous methods have been developed to prepare CdS nanocrystalline films, typically physical vapor deposition [20–22], magnetic sputtering [23], close spaced sublimation [24], molecular beam epitaxy [25], chemical vapor deposition [26], chemical bath deposition (CBD) [27,28], electrodeposition [29], successive ionic layer adsorption and reaction (SILAR) method [30–32], photochemical deposition [33], screen printing [34], electrostatic assisted aerosol jet deposition [35] and ion layer gas reaction (ILGAR) method [36]. Recent years, there have been increasing efforts in developing new synthesis techniques which particularly have some advantages on green materials, low cost and easy fabrication on a large scale. CBD is a time-efficient method and can deposit high quality CdS thin films on large area substrates. However, the homogeneous nucleation in the reaction solution, which simultaneously was accompanied with the effective heterogeneous nucleation deposition on substrate for thin film formation, took place in the deposition solution, leading to a high proportion of Cd and S precursor source loss and further environmental pollution [26,27]. SILAR is a simple, low cost and less precursor source loss preparation but it is of low time-efficiency and only has about 2–3 nm deposited layer thickness per SILAR cycle [29,30]. So, we suggested whether a new deposition method could be developed, which used SILAR deposition cycles with improved time-efficiency by displacing the thin ion-absorbed layer with a pre-formed and thick cationic precursor solid film. In this work, we described the new synthesis method, named in situ chemical reaction synthesis, to prepare CdS thin films. The method used pre-formed cadmium nitrate solid thin films as cationic reaction source and sodium sulfide based solutions as anionic reaction medium. The effects of anionic concentration, in situ deposition temperature and annealing treatment on crystallization, morphology, stoichiometry and optical properties of the CdS thin films by the in situ chemical reaction synthesis were mainly investigated by X-ray diffraction (XRD), field emission scanning electron microscope (FESEM), energy dispersive X-ray analyzer (EDAX) and UV–Vis spectra measurement.

* Corresponding author. Fax: +86 22 27404724.
E-mail address: zhgjin@tju.edu.cn (Z. Jin).

0925-8388/$ – see front matter © 2011 Elsevier B.V. All rights reserved.
doi:10.1016/j.jallcom.2011.11.141

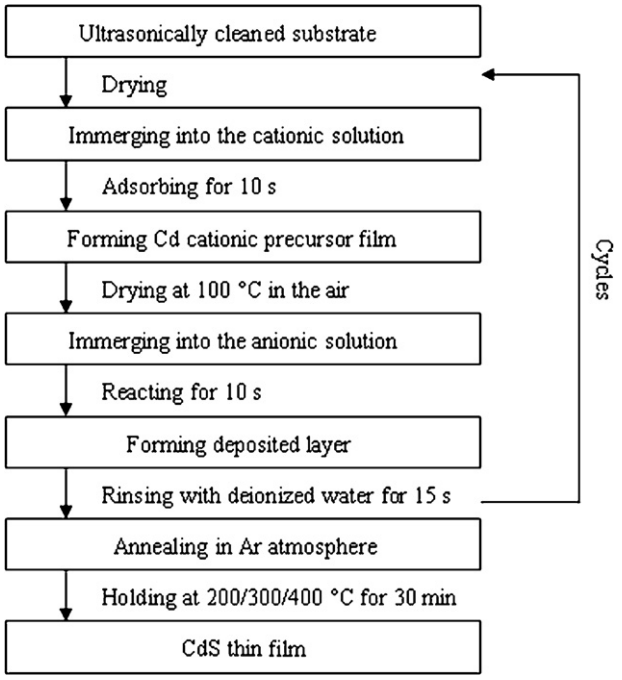

Fig. 1. Flow chart of CdS thin film by in situ chemical reaction process.

2. Experimental

2.1. Chemicals

For in situ deposition of CdS thin films, the following chemicals were used: cadmium nitrate ($Cd(NO_3)_2{\cdot}4H_2O$), sodium sulfide (Na_2S), ethylene glycol monomethylether ($HO(CH_2)_2OCH_3$), butyl alcohol ($CH_3(CH_2)_3OH$), ethanolamine ($HO(CH_2)_2NH_2$) and deionized water. All chemicals are AR grade and directly used.

2.2. Preparation of CdS thin films

Cationic solution for the pre-formed Cd precursor films: 0.15 M $Cd(NO_3)_2{\cdot}4H_2O$ was dissolved into a mixed solution of 15 mL ethylene glycol monomethylether, 3 mL ethanolamine and 2 mL butyl alcohol. Anionic reaction solutions: certain content of Na_2S was dissolved into a mixed solution of 12 mL deionized water and 8 mL ethylene glycol monomethylether, and the Na_2S concentrations were 0.15, 0.30, 0.45 and 0.60 M, respectively. The CdS films were respectively deposited in the four different anionic reaction solutions at solution temperature of 20 °C. To investigate effect of in situ deposition temperature, deposition temperature was altered at 20 °C, 40 °C and 60 °C, respectively, with the fixed Na_2S concentration of 0.30 M. Microscope glass slides of 25 mm × 15 mm × 1 mm were used as substrates, which were ultrasonically cleaned with 30% nitric acid, alcohol and deionized water for 20 min, respectively. The flow chart of preparation of CdS thin films by the in situ chemical reaction process is shown in Fig. 1. At first, Cd^{2+} precursor solid thin films were coated on cleaned glass substrates by dip-drawing method and following drying at oven of 100 °C in the air. Then the coated substrates were immersed into anionic reaction solution for 10 s, where Cd^{2+} reacted with S^{2-} to generate CdS deposited layer. The substrate was washed with deionized water for 15 s to remove counter ions and organic impurity. Above operation cycle was repeated for 2–10 times to investigate film growth. The as-deposited films were annealed at temperatures of 200 °C, 300 °C and 400 °C for 30 min in argon atmosphere, respectively. The processing conditions used in the experiment are listed in Table 1. The chemical reaction formulae involved in the in situ reaction process are given as follows:

$$Cd(NO_3)_2 \rightarrow Cd^{2+} + 2NO_3^- \quad (1)$$

$$Cd^{2+} + n\,HO(CH_2)_2NH_2 \rightarrow Cd[O(CH2)_2NH_2]_n^{2-n} \quad (2)$$

$$Na_2S \rightarrow 2Na^+ + S^{2-} \quad (3)$$

$$Cd[O(CH2)_2NH_2]_n^{2-n} + S^{2-} \rightarrow CdS + n\,HO(CH_2)_2NH_2 \quad (4)$$

2.3. Characterization

X-ray diffraction analysis was carried out using a Rigaku D/Max 2500V/PC X-ray powder diffractometer with CuKα radiation (λ = 1.54178 Å) at a scanning rate of 8°/min ranging from 2θ = 10° to 80°. The surface morphologies and cross section of CdS thin films were observed by Hatchi S-4800 model field emission scanning electron microscope, and the accelerating voltage is 10 kV. The chemical composition of CdS thin film was determined by energy dispersive X-ray analysis (EDAX) using a Genesis XM2 energy dispersive X-ray analyzer attached FESEM. The optical absorption spectra were recorded using TU-1901 UV–Vis spectrophotometer ranging from 200 to 900 nm.

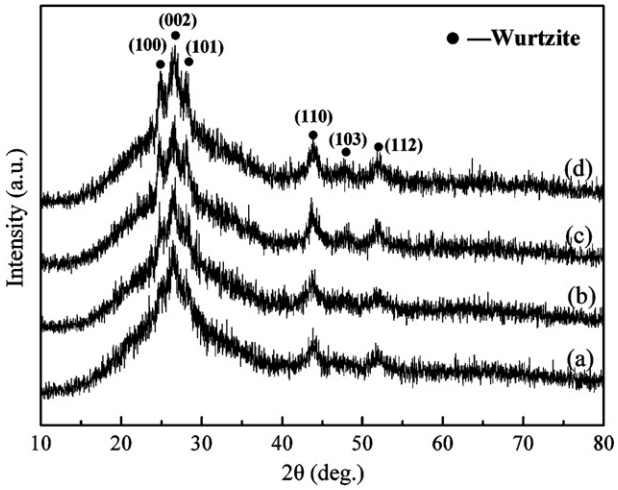

Fig. 2. XRD patterns of CdS thin films deposited with Na_2S concentrations of (a) 0.15 M, (b) 0.30 M, (c) 0.45 M and (d) 0.60 M at 20 °C, 10 dip-cycles and annealed at 200 °C in Ar.

3. Results and discussion

3.1. Influence of Na_2S concentration

Fig. 2 shows the X-ray diffraction patterns of the nano-crystalline CdS thin films deposited with Na_2S concentrations of (a) 0.15 M, (b) 0.30 M, (c) 0.45 M and (d) 0.60 M, respectively, at 20 °C, 10 dip-cycles and annealed at 200 °C in Ar. It is seen that the diffraction patterns are at early stage crystallization of hexagonal wurtzite structure (JCPDS, 41-1049), and the three major peaks at 2θ of 26.5°, 43.2° and 51.9° can be assigned to (0 0 2), (1 1 0) and (1 1 2) planes of the hexagonal phase. With increasing S:Cd molar concentration to 0.30:0.15, another two peaks at 24.9° and 28.2° appear in Fig. 2(b), which can be assigned to plane (1 0 0) and (1 0 1) reflection of hexagonal wurtzite phase. The two characteristic peaks become more definite for the film sample with S:Cd molar concentration of 0.45:0.15 meanwhile the peak at 2θ = 47.8°, corresponding the hexagonal (1 0 3) plane, is also seen in Fig. 2(c). Fig. 2(d) is the XRD pattern of CdS thin film deposited at S:Cd molar concentration of 0.60:0.15, showing that the six main peaks become sharper than the former. So, it can be concluded that the intensities of diffraction peaks increase with rising anionic concentration, which means that the increase of Na_2S concentration has a role on increasing crystallinity of the deposited layer. The Scherrer's relation is used to calculate crystallite size of the CdS thin films:

$$D = \frac{0.94\lambda}{\beta \cos\theta} \quad (5)$$

where λ is the wavelength of incident X-ray, θ is the diffracted angle and β is the full width at the half maximum height. The crystallite size of all the four samples is in the range of 11–12 nm.

Fig. 3 is the X-ray diffraction patterns of the nano-crystalline CdS thin films deposited with Na_2S concentrations of (a) 0.15 M, (b) 0.30 M, (c) 0.45 M and (d) 0.60 M, respectively, at 20 °C, 10 dip-cycles and annealed at 400 °C in Ar. It is seen that the hexagonal wurtzite diffraction peaks of all the films annealed at 400 °C become sharper when compared with those of the samples annealed at 200 °C. Particularly, the intensities of three main peaks of (1 0 0), (0 0 2) and (1 0 1) planes in the XRD patterns are not in agreement

Table 1
Processing condition for deposition of CdS thin films.

Parameters	Cationic precursor (mol/L)	Anionic precursor (mol/L)
Sources	Cadmium nitrate	Sodium sulfide
Concentration (M)	0.15	0.15/0.30/0.45/0.60
Immersion time (s)	10	10
Immersion cycles (n)	2/4/6/8/10	2/4/6/8/10
Solution temperature (°C)	20	20/40/60
Annealing temperature (°C)	200/300/400	

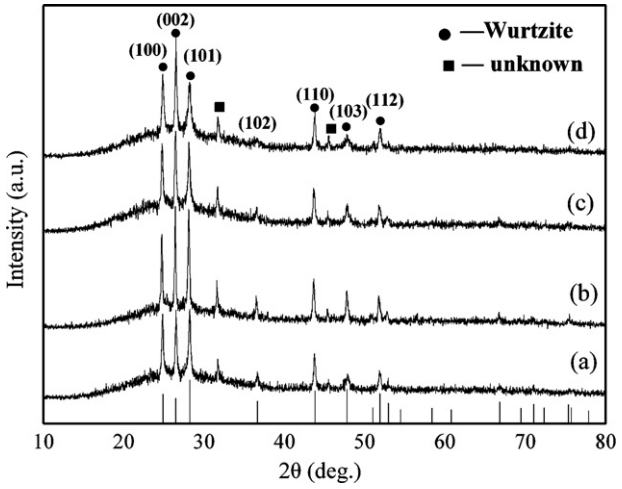

Fig. 3. XRD patterns of CdS thin films deposited with Na_2S concentrations: (a) 0.15 M, (b) 0.30 M, (c) 0.45 M and (d) 0.60 M at 20 °C, 10 dip-cycles and annealed at 400 °C in Ar.

with those of the standard JCPDS card found at the bottom of this Fig. 3. The (0 0 2) preferred orientation is clearly seen and gradually enhanced with increase of S:Cd molar concentration ratio. It indicates that quick nucleation and crystal growth rate tends to encourage the (0 0 2) preferred orientation as S:Cd molar concentration ratio is high in the in situ reaction deposition. In addition, there are two unknown peaks at 31.8° and 45.3° after annealing, which might be induced by sodium-containing impurities, not indexed to any JCPDS standard card. The Scherrer's relation is used again to calculate crystallite size of the films annealed at 400 °C in Ar. They are 26, 36, 36 and 36 nm respectively, showing that annealing at higher temperature promotes crystallite growth and improved crystallinity of the CdS thin films considerably.

The surface morphologies of CdS thin films with different anionic concentrations of 0.15, 0.30, 0.45 and 0.60 M respectively, and 10 dip-cycles and annealed at 200 °C in Ar are shown in Fig. 4. As is shown in Fig. 4(a), the film with 0.15 M anionic concentration is not very flat and compact. The film morphologies of Fig. 4(b)–(d) are better than that of Fig. 4(a). It indicates that the morphology could be improved by relatively uniform deposition growth when the anionic concentration increased. Grain sizes of the four samples by the FESEM observation are almost the same without obvious difference, ranging from 20 to 23 nm.

Fig. 5 is an EDAX spectrum of the CdS thin film prepared with molar concentration of S:Cd = 0.15:0.15 M in separate precursor solutions, and at deposition temperature of 20 °C, 10 dip-cycles and annealed at 300 °C in Ar. It shows that the film contains the elements Cd and S as deposited components and S/Cd atomic ratio is 1.04. Some impurity elements such as Si, Al, Na, O, C, N and Au were also detected by EDAX. Among these elements, Si, Al, Na and partly O are attributed to the chemical components of glass substrate. C, O and N are due to exposure to the atmosphere and residual elements from the organic chemicals of precursor solution. Au is due to golden coat on the in situ deposited CdS thin films for FESEM observation. The S/Cd atomic ratios of CdS thin films deposited at different annealing temperatures and molar concentrations analyzed by EDAX are showed in Table 2. It can be seen that with the increase of anionic solution concentration, the S:Cd atomic ratios on films also increased. In addition, with the increase of annealing temperature, the S:Cd atomic ratios on films are decreased when the

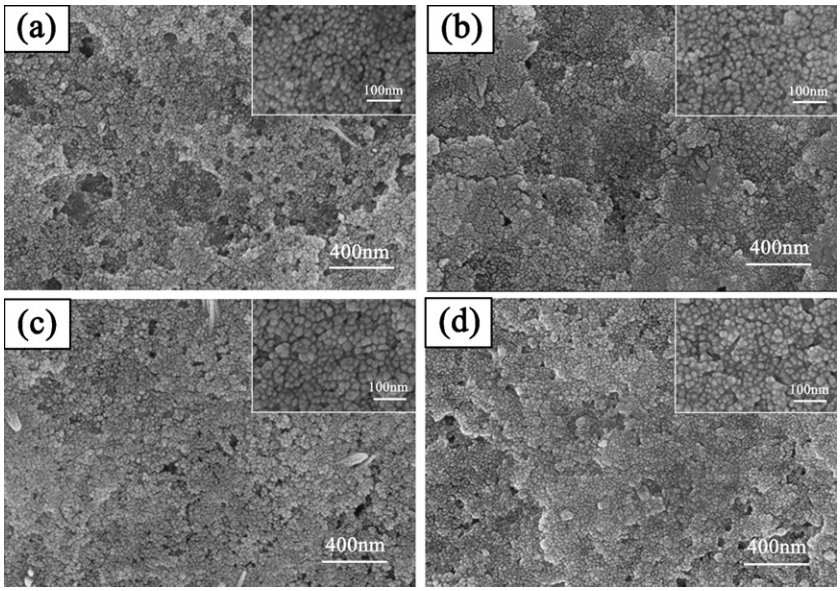

Fig. 4. FESEM micrographs of CdS thin films deposited with different Na_2S concentrations of (a) 0.15 M, (b) 0.30 M, (c) 0.45 M, (d) 0.60 M and 10 dip-cycles and annealed at 200 °C in Ar.

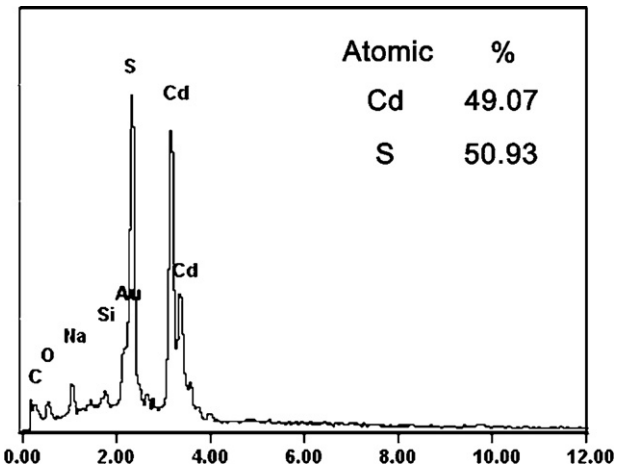

Fig. 5. EDAX spectrum of the CdS thin film prepared with molar concentration of S:Cd = 0.15:0.15 M in separate precursor solutions and 10 dip-cycles.

molar concentration of S:Cd in separate precursor solutions were fixed, which may be caused by volatilization of element S on the films during heat treatment.

Fig. 6 shows optical absorption spectra of the CdS films deposited with Na_2S concentrations of 0.15, 0.30, 0.45, 0.60 M respectively, 4 dip-cycles and annealed at 200 °C in Ar. All these absorption spectra show a shoulder peak at 476–482 nm and slightly blue shift compared with the reported data of 512 nm for bulk CdS. This blue shift does not be attributed to the nanosize effect because the Bohr radius of CdS is 6 nm, smaller than the average crystallite size 11–12 nm calculated by the Scherrer's relation for the in situ synthesized CdS films. Using the standard expression for direct transition between two parabolic bands $(\alpha h\nu)^{1/n} = A(h\nu - E_g)$, where A is a constant related to the effective masses associated with the bands and $n = 1/2$ for a direct-gap material, the band gap E_g of the investigated CdS layers were determined by extrapolating the linear $(\alpha h\nu)^2$ versus $h\nu$ plots to the energy axis shown in Fig. 7. It is seen that the direct band gap energies are smaller than the values of 2.42 eV for single crystal and decrease with the increase of Na_2S concentration in a narrow range of 2.30–2.34 eV. The results should be related to microstructure imperfection, surface and lattice defects of the CdS thin films [37]. The regularly reduced band gaps with increasing Na_2S concentration may also be caused by deviation out of the Cd:S = 1 stoichiometry, which induced lattice faults at non-stoichiometric situation, all leading to the red shift.

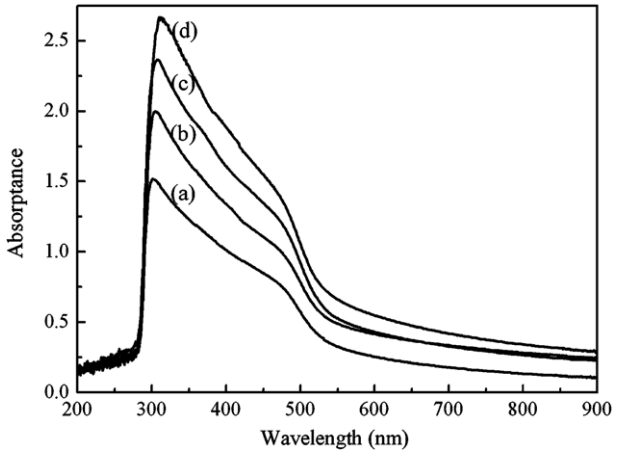

Fig. 6. Optical absorption spectra of CdS thin films deposited with different Na_2S concentrations: (a) 0.15 M, (b) 0.30 M, (c) 0.45 M, (d) 0.60 M and 4 dip-cycles and annealed at 200 °C in Ar.

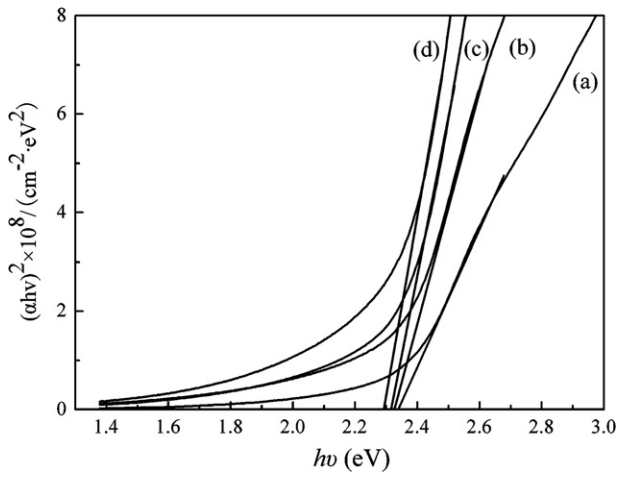

Fig. 7. $(\alpha h\nu)^2$ versus $(h\nu)$ plots of CdS thin films deposited with different Na_2S concentrations: (a) 0.15 M, (b) 0.30 M, (c) 0.45 M, (d) 0.60 M and 4 dip-cycles and annealed at 200 °C in Ar.

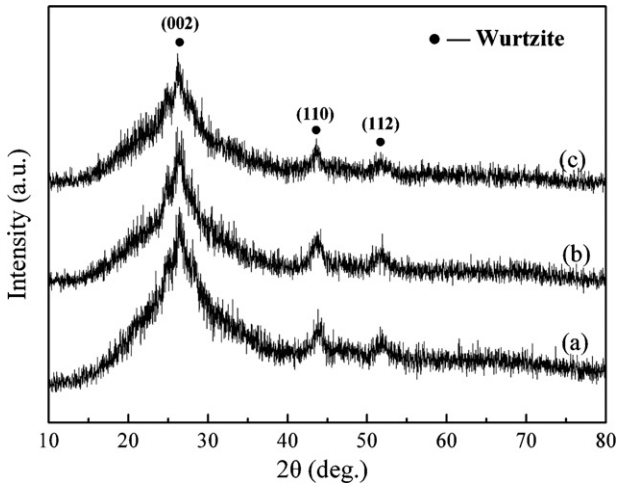

Fig. 8. XRD patterns of CdS thin films deposited at different temperatures: (a) 20 °C, (b) 40 °C, (c) 60 °C, and with 10 dip-cycles and annealed at 200 °C in Ar.

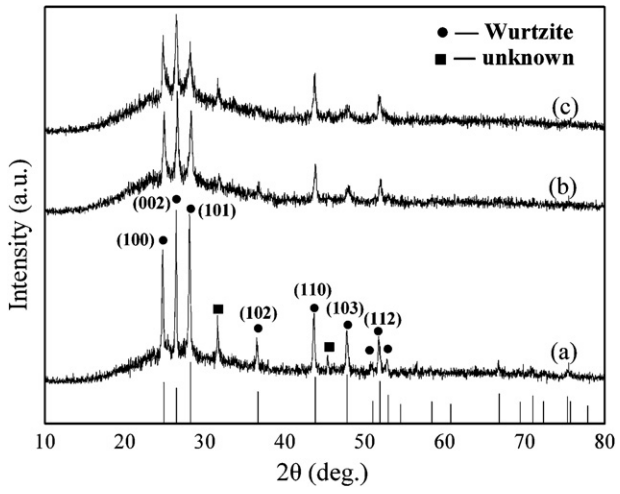

Fig. 9. XRD patterns of CdS thin films deposited at different temperatures: (a) 20 °C, (b) 40 °C, (c) 60 °C, and with 10 dip-cycles and annealed at 400 °C in Ar.

Table 2
EDAX analysis on surface of CdS thin films prepared with different processing conditions.

S:Cd atomic ratios on surface of CdS thin films				
Annealing temperature (°C)	Molar concentrations of S:Cd in separate precursor solutions			
	0.15:0.15	0.30:0.15	0.45:0.15	0.60:0.15
200	1.07	1.17	1.24	1.29
300	1.04	1.14	1.21	1.25
400	1.02	1.11	1.19	1.23

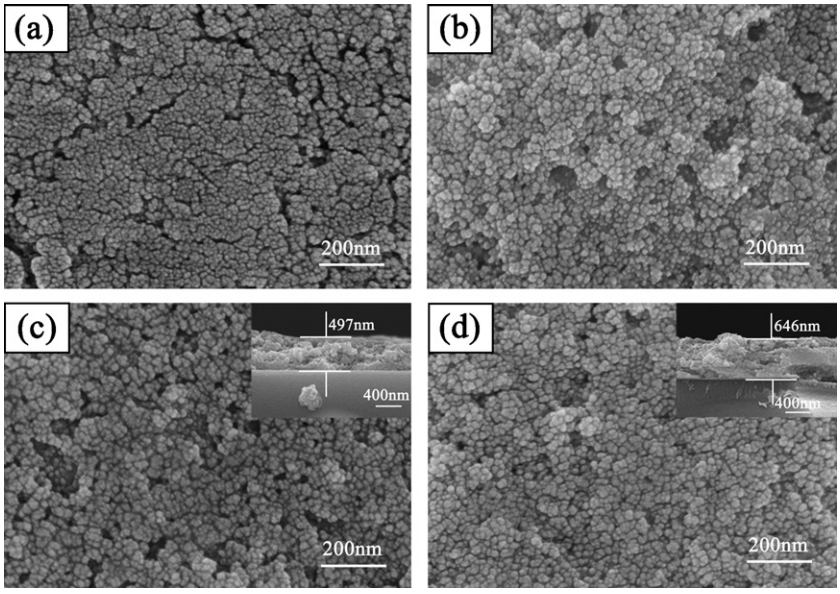

Fig. 10. Surface and cross section morphologies of CdS thin films with different reaction cycles of (a) 2, (b) 4, (c) 6 and (d) 8, deposited at 20 °C and annealed at 200 °C.

3.2. In situ deposition temperatures

In order to explore effect of in situ deposition temperature, CdS films were deposited at different reaction solution temperatures of 20 °C, 40 °C, 60 °C respectively, and different cycle numbers of 2–10 and fixed the S/Cd ratio 0.30:0.15 in starting separate precursor solution. Fig. 8 shows XRD patterns of the CdS thin films deposited at 20 °C, 40 °C, 60 °C, and with 10 dip-cycles and annealed at 200 °C in Ar. The peaks at $2\theta = 26.5°$, 43.2° and 51.9° correspond to the (0 0 2), (1 1 0) and (1 1 2) planes of hexagonal wurtzite phase, respectively. Also, it is seen that the crystallization degree of CdS films is almost unchanged with the increase of in situ deposition temperature. The Scherrer's relation was used to calculate crystallite size of the films annealed at temperatures of 200 °C in Ar,

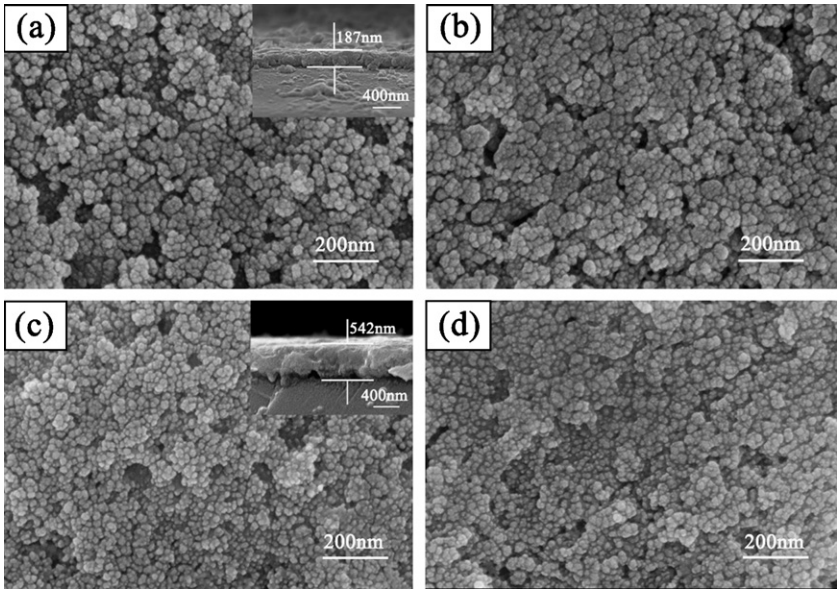

Fig. 11. Surface and cross section morphologies of CdS thin films with different reaction cycles of (a) 2, (b) 4, (c) 6 and (d) 8, deposited at 40 °C and annealed at 200 °C.

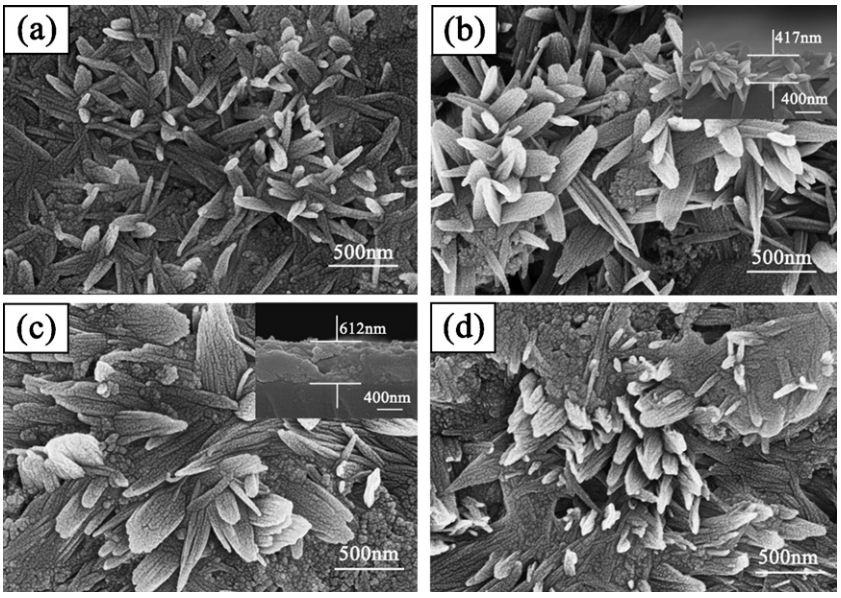

Fig. 12. Surface and cross section morphologies of CdS thin films with different reaction cycles of (a) 2, (b) 4, (c) 6 and (d) 8, deposited at 60 °C and annealed at 200 °C.

and they were in the range of 11–12 nm. For the CdS thin film annealed at 400 °C, the characteristic peaks at 24.8° and 28.2° appear besides the three peaks, which can be assigned to plane (1 0 0) and (1 0 1) reflection of hexagonal wurtzite phase. Moreover, it is seen from Fig. 9 that the crystallization degree of the CdS thin films annealed at 400 °C decreases with increase of in situ deposition temperature. The peak at $2\theta = 36.6°$, corresponding to the hexagonal (1 0 2) plane, becomes weak and even disappears with increase of in situ deposition temperatures. The Scherrer's relation was used again to calculate crystallite size of the films annealed at 400 °C in Ar, and they were 36, 30 and 26 nm, respectively, gradually reduced with the increase of in situ deposition temperatures.

Figs. 10–12 show surface and cross section morphologies of CdS films obtained under different deposited conditions. From Fig. 10, it can be seen that the thin films become flat and dense with the increase of cycle numbers. The grain size gradually increases from 16 nm with 2 dip-cycles to 23 nm with 8 dip-cycles. The thickness of thin films with 6 dip-cycles and 8 dip-cycles was 497 nm and 646 nm respectively, implying that growth rate of film thickness prepared at 20 °C is about 82 nm per cycle. Fig. 11 shows the surface and cross section morphologies of CdS thin films deposited at 40 °C. The particle size enlarges to 25 nm on the average, and granulated deposits become clear and surface evolves uneven with rising deposition temperature. The film thickness increases from 187 nm with 2 dip-cycles to 542 nm with 6 dip-cycles, corresponding to thickness growth rate of 92 nm per cycle. From Fig. 12, it can be seen that at deposition temperature 60 °C, growth rate was so fast that the CdS crystal nucleus could not form particle and tended to grow epitaxially to form flower-like nanostructured CdS on films. The thickness of films deposited at 60 °C was ranged from 417 nm with 4 dip-cycles to 612 nm with 6 dip-cycles, indicating that its growth rate is 103 nm per cycle. It is known that ionic diffusion velocity, ionic adsorption and desorption, and reaction kinetics of adsorbed cations with anions to form sulfide compound are all related to deposition temperature. Deposition temperature dominantly affected synthetic reaction kinetics and ionic diffusion velocity for the process of deposition [37]. So, it can be concluded that high reaction kinetics and ionic diffusion velocity at elevated temperature can contribute to fast growth rate.

4. Conclusions

Wurtzite CdS nanocrystalline thin films could be deposited on glass substrates by the in situ chemical reaction synthesis using cadmium precursor solid films as reaction source and sodium sulfide based solutions as anionic reaction medium. The characterization studies reveal that S:Cd concentration ratios in the starting separate precursor solutions had influence on the crystalline structure, morphologies, chemical composition and optical properties of the deposited CdS films. The SEM images showed that the films became more homogeneous with increase of the S:Cd molar concentration ratio, but EADX analysis showed that S:Cd atomic ratio of the grown films was increased with rising the molar concentration ratio in separate precursor solution. The optical absorption spectra had a shoulder peak at 476–482 nm of absorption edge and the optical band gap energies were in the range of 2.30–2.34 eV. The increase of deposition temperature could cause fast growth, large particle size, and even flower-like film morphology. The deposition rate was 80–100 nm thickness per cycle in the range of deposition temperature from 20 °C to 60 °C.

Acknowledgements

The authors acknowledge financial supports from the State Key Laboratory of Silicon Materials at Zhejiang University (Project No. SKL2010-11) and the Key Laboratory for Advanced Ceramics and Machining Technology of Ministry of Education at Tianjin University (Project No. ACMT201001).

References

[1] H.R. Moutinho, D. Albin, Y. Yan, R.G. Dhere, X. Li, C. Perkins, C.S. Jiang, B. To, M.M. Al-Jassim, Thin Solid Films 436 (2003) 175–180.
[2] H. Metin, R. Esen, Semicond. Sci. Technol. 18 (2003) 647–654.
[3] V. Popescu, E.M. Pica, I. Pop, R. Grecu, Thin Solid Films 349 (1999) 67–70.
[4] Y.H. Lee, W.J. Lee, Y.S. Kwon, G.Y. Yeom, J.K. Yoon, Thin Solid Films 341 (1999) 172–175.
[5] S. Kumazawa, S. Shibutani, T. Nishio, T. Aramoto, H. Higuchi, T. Arita, A. Hanafusa, K. Omura, M. Murozono, H. Takakura, Sol. Energy Mater. Sol. Cells 49 (1997) 205–212.
[6] T. Vossmeyer, L. Katsikas, M. Giersig, I.G. Popovic, K. Diesner, A. Chemseddine, A. Eychmueller, H. Weller, J. Phys. Chem. 98 (1994) 7665–7673.
[7] Y. Hashimoto, N. Kohara, T. Negami, N. Nishitani, T. Wada, Sol. Energy Mater. Sol. Cells 50 (1998) 71–77.

[8] T. Maruyama, R. Kitamura, Sol. Energy Mater. Sol. Cells 69 (2001) 61–68.
[9] M. Tsuji, T. Aramoto, H. Ohyama, T. Hibino, K. Omura, J. Cryst. Growth 214/215 (2000) 1142–1147.
[10] U. Rau, H.W. Schock, Appl. Phys. A 69 (1999) 131–147.
[11] M. Bar, L. Weinhardt, C. Heske, H.-J. Muffler, E. Umbach, M.Ch. Lux-Steiner, Th.P. Niesen, F. Karg, Ch.-H. Fischer, Sol. Energy Mater. Sol. Cells 90 (2006) 3151–3157.
[12] V.I. Klimov, A.A. Mikhailovsky, S. Xu, A. Malko, J.A. Hollingsworth, C.A. Leatherdale, H.-J. Eisler, M.G. Bawendi, Science 290 (2000) 314–317.
[13] M.Jr. Bruchez, M. Moronne, P. Gin, S. Weiss, A.P. Alivisatos, Science 281 (1998) 2013–2016.
[14] W.J. Parak, D. Gerion, T. Pellegrino, D. Zanchet, C. Micheel, S.C. Williams, R. Boudreau, M.A. Le Gros, C.A. Larabell, A.P. Alivisatos, Nanotechnology 14 (2003) R15–R27.
[15] J.A.B. Howie, G.K. Rowles, P. Hawkins, Meas. Sci. Technol. 2 (1991) 1070–1073.
[16] T.L. Chu, S.S. Chu, Prog. Photovolt. Res. Appl. 1 (1993) 31–42.
[17] A. Fuijishima, K. Honda, Nature 238 (1972) 37–38.
[18] H.M. Jia, Y. Hu, Y.W. Tang, L.Zh. Zhang, Electrochem. Commun. 8 (2006) 1381–1385.
[19] H. Fujii, M. Ohtaki, K. Eguchi, H. Arai, J. Mol. Catal. A: Chem. 129 (1998) 61–68.
[20] R.W. Birkmire, B.E. McCandless, S.S. Hegedus, Int. J. Solar Energy 12 (1992) 145–149.
[21] J.H. Lee, W.C. Song, J.S. Yi, K.J. Yang, W.D. Han, J. Hwang, Thin Solid Films 431 (2003) 349–353.
[22] P.D. Persans, L.B. Lurio, J. Pant, G.D. Lian, T.M. Hayes, Phys. Rev. B 63 (2001) 115320.
[23] S. Bonilla, E.A. Dalchiele, Thin Solid Films 204 (1991) 397–403.
[24] T.L. Chu, S.S. Chu, J. Britt, C. Frekides, C. Wang, C.Q. Wu, IEEE Trans. Electron Device Lett. 13 (1992) 303–304.
[25] K.B. Ozanyan, J.E. Nicholls, L. May, J.H.C. Hogg, W.E. Hagston, B. Lunn, D.E. Ashenford, Solid State Commun. 99 (1996) 407–411.
[26] K.C. Chou, A. Rohatgi, J. Electron. Mater. 23 (1994) 31–37.
[27] K. Durose, P.R. Edwards, D.P. Halliday, J. Cryst. Growth 179 (1999) 733–742.
[28] M.A. Martinez, C. Guillen, J. Herrenro, Appl. Surf. Sci. 140 (1999) 182–189.
[29] G. Sasikala, R. Dhnasekaran, C. Subramanian, Thin Solid Films 302 (1997) 71–76.
[30] M.P. Valkonen, S. Lindroos, T. Kanniainen, M. Leskela, U. Tapper, E. Kauppinen, Appl. Surf. Sci. 120 (1997) 58–64.
[31] Y.F. Nicolau, Appl. Surf. Sci. 22/23 (1985) 1061–1074.
[32] X.X. Liu, Z.G. Jin, S.J. Bu, J. Zhao, Z.J. Cheng, J. Inorg. Mater. 19 (2004) 691–695.
[33] F. Goto, M. Ichimura, E. Arai, J. Appl. Phys. 36 (1997) 1146–1149.
[34] S.A. Al Kuhaimi, Vacuum 51 (1998) 349–355.
[35] B. Su, M. Wei, K.L. Choy, Mater. Lett. 47 (2001) 83–88.
[36] J.J. Qiu, Z.G. Jin, W.B. Wu, X.X. Liu, Z.J. Cheng, Rare Met. 23 (2004) 311–316.
[37] J.X. Yang, Z.G. Jin, Y. Chai, H. Du, T. Liu, T. Wang, Thin Solid Films 517 (2009) 6617–6622.